IL NUOVO CIMENTO Vol. 32 C, N. 1 Gennaio-Febbraio 2009
DOI 10.1393/ncc/i2009-10355-2

Colloquia: GCM8

New developments in topological fluid mechanics

Renzo L. Ricca(*)

Dipartimento di Matematica e Applicazioni, Università di Milano-Bicocca
Via Cozzi 53, 20125 Milano, Italy

(ricevuto il 3 Aprile 2009; pubblicato online il 20 Luglio 2009)

Summary. — In this paper we present and discuss ideas and new results in three different research areas of topological fluid mechanics. First, we propose a conjectured experiment to produce and observe, for the first time, vortex knotting in real fluids. Next we provide a new ropelength bound for tight, magnetic knots in ideal magnetohydrodynamics. Finally, we present a novel interpretation of eigenvalue analysis of tensor fields in terms of integral geometry by using the information on form factors provided by structural complexity analysis.

PACS 11.10.-z – Field theory.
PACS 47.10.A- – Mathematical formulations.
PACS 47.32.C- – Vortex dynamics.
PACS 52.30.Cv – Magnetohydrodynamics (including electron magnetohydrodynamics).

1. – Introduction

Helmholtz's seminal paper on vortex motion (1858) marks the beginning of what is now called topological fluid mechanics [1]. After 150 years of work the field has grown considerably, but it is only in the last fifteen years that has seen new, interesting and unexpected developments. With this paper we want to present and discuss ideas and new results that are at the core of current research. First, we shall start from an old and outstanding problem of classical vortex dynamics, namely the production and observation of vortex knotting. We shall propose a conjectured experiment, that relies on advancements in analytical and computational work, aimed at detecting vortex knotting under controlled conditions in the laboratory. This should provide a stimulating challenge to both experimentalists and numerical analysts. Next we shall present new results on the groundstate energy of magnetic knots in ideal magnetohydrodynamics, in relation to current work on ropelength of ideal knots, thus providing a new ropelength bound for tight, magnetic knots, and possible clues to make further progress in topological field theory and knot classification. Finally, in the last section, we shall consider measures of

(*) E-mail: renzo.ricca@unimib.it — URL: http://www.matapp.unimib.it/~ricca

integral geometry for the morphological analysis of distribution sets, by providing a novel interpretation of eigenvalue analysis of tensor fields in terms of form factors of structural complexity. These results are representative of a very small fraction of current work in topological fluid mechanics. Nevertheless, with these three cases we provide an example of the richness and variety of current research.

2. – A conjectured experiment on vortex knotting

Real vortex dynamics is inherently a three-dimensional process that involves interaction, reconnection and continuous re-organization of vortical structures in the fluid. For this reason vortex tube reconnection represents a prototype example [2, 3], and it is of fundamental importance to analyze and understand energy transfer and dissipation to smaller scales. Upon reconnection vortex topology changes and this entails a change in the kinetic helicity of the system due to a local exchange of writhe and twist helicity in the interacting tube strands [4]. These are clearly key mechanisms to understand energy decay in real fluids, but so far very little work has been done to investigate these aspects from an experimental viewpoint.

Here we propose a conceptually simple experiment to study these properties through the production and evolution of a real vortex knot. Here vortex knotting is conjectured on the basis of a numerical simulation of vortex linking [5]. The envisaged process is shown in fig. 1, where knotting is produced through the interaction and reconnection of two vortex rings, represented in fig. 1 by the projected diagrams of the ring axes. The initial condition is shown in fig. 1a, where two nearly planar, parallel vortex rings (numbered by 1 and 2) are shot co-axially one after the other, at times t_1 and t_2, respectively. Both vortex rings are given by a 3-mode perturbation from the circular vortex ring: in a coordinate system co-moving with the centre of mass of the ring, the 3-mode perturbation ring may be prescribed according to [6] by

$$\mathbf{X} = (R + re^{im\theta})\hat{\mathbf{e}}_r + ze^{im\theta}\hat{\mathbf{e}}_z, \tag{1}$$

where $\hat{\mathbf{e}}_r$ and $\hat{\mathbf{e}}_z$ are unit vectors in the radial and axial direction of the ring, θ is the azimuthal angle, R is the radius of the unperturbed ring and $\{r, z\} \ll R$. The wave number m is an integer with $m = 1, 2, 3, \ldots$. A linear perturbation analysis demonstrates that for moderate values of m the ring oscillates with an angular frequency $\pm\alpha_m$. In the case $m = 2$, the two solutions can be superposed to give a planar elliptic form; similarly, for $m = 3$ we obtain the 3-mode planar perturbation shown in fig. 1a. This provides useful information for designing the orifice aperture. By using the value of α_3 given by Widnall and Sullivan [6], we can also get information on vortex core radius and vorticity distribution.

Once shot, the two vortex rings interact and deform by mutual induction (see fig. 1b) according to the Biot-Savart law. Reconnections are triggered at specific locations when the tube strands are at a distance of the order of the vortex core diameter and are mutually inclined at an angle below about 35°. It is well known [7] that thin vortex filaments move in the fluid with a velocity that, to leading order, is given by a curvature contribution in the binormal direction, plus a rotational contribution around a core axis; the first contribution is associated with the the so-called Localized Induction Approximation (LIA for short) law, given by

$$\mathbf{u}_{\mathrm{LIA}} = \frac{\Gamma c}{4\pi} \ln \delta \, \hat{\mathbf{b}} \propto c\hat{\mathbf{b}}, \tag{2}$$

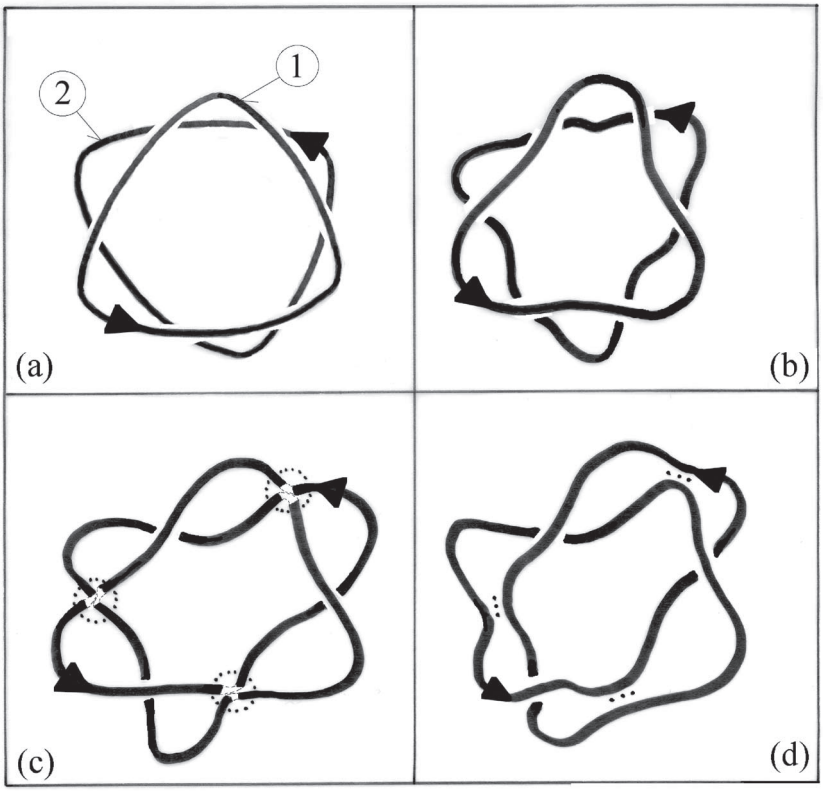

Fig. 1. – A conjectured experiment of vortex knotting produced by interaction and reconnection of two 3-mode perturbation vortex rings. Diagrams show the conjectured time evolution of the projected vortex axes: (a) initial configuration; (b) mutual interaction and deformation; (c) local reconnections; (d) emergence of trefoil knotting.

where Γ is the vortex circulation, c is the local curvature, δ is a measure of the aspect ratio of the vortex, and $\hat{\mathbf{b}}$ is the local unit binormal. From the right-hand side of eq. (2) we see that the local dynamics is indeed dictated by curvature information. Since curvature is higher at the 3 apices of the 3-mode perturbation ring, these regions will move away with higher speed, leaving behind the three intermediate regions of low concavity. Since the same applies to both rings, ring 2 must be rotated by an angle θ_0 to enable its concave regions to catch-up and reconnect with the neighbouring parts of ring 1 (fig. 1c). Moreover, since each vortex induces a rotational flow around its axis, vortex elements will be bent away from the original plane of embedding, by rotating around each other.

To estimate the time lapse $\Delta t = t_2 - t_1$ between the two consecutive shots and the mutual angle θ_0 (and hence the reconnection time) we may take advantage of the perturbation analysis made on LIA by Arms and Hama [8]; for $m = 3$, we have

$$r = a\cos\frac{6\sqrt{2}}{R^2}t\,\cos 3\theta, \qquad z = a\frac{2\sqrt{2}}{3}\sin\frac{6\sqrt{2}}{R^2}t\,\cos 3\theta, \tag{3}$$

where $a \ll R$. Equations (3) provide the time evolution of the 3-mode perturbation

from the circular ring of radius R. Since the resulting motion is given by a combination of a translation along $\hat{\mathbf{e}}_z$ and a rotation around the z-axis, from the second of (3) we can estimate Δt and from the first θ_0. The curvature c of the 3-mode perturbed ring is given by

$$c = R^{-1}\left[1 - \frac{8a}{R}\cos\frac{6\sqrt{2}}{R^2}t + O\left(\frac{a}{R}\right)^2\right]^{-1}; \tag{4}$$

since curvature information is directly related to the propagation velocity (see eq. (2)), by the above equation and information on Δt we can estimate the distance between rings 1 and 2. Upon reconnection, a trefoil knot may be produced as shown in fig. 1(d). If the emergent knot is sufficiently intense (compared to diffusivity), LIA stability results [9] ensure that for small-amplitude perturbations the vortex knot would be relatively long lived. However, as vortex ring experiments amply demonstrate, high accuracy in the shooting mechanism and in engineering the orifice will be necessary to control as much as possible the emergence of Kelvin wave instabilities and wake disturbances in order to prevent vortex decoherence and immediate decay.

3. – New ropelength bound for tight, magnetic knots

Work on groundstate energy of magnetic knots [10] has revealed new connections between magnetic relaxation of flux-tubes and ropelength of tight, ideal knots (see, for example, [11]). Let K be a magnetic knot of tube axis $\mathcal{C}$ and circular cross-section $\mathcal{S}$. The magnetic field is given by $\mathbf{B} = (0, B_\theta, B_s)$, where $B_\theta = B_\theta(r)$ and $B_s = B_s(r)$ are the poloidal and toroidal components in a local cylindrical, polar coordinate system (r, θ, s) centred on $\mathcal{C}$. The knot K, of volume V, length L and magnetic flux Φ, is embedded in an ideal fluid and relaxes under the action of the Lorentz force, to attain a minimum energy configuration. Magnetic relaxation takes place under volume and flux conservation, and the energy minimum is constrained by the topology of K (see fig. 2). In recent work Maggioni and Ricca [12] demonstrate that for standard flux-tube minimization of magnetic energy subject to the invariance of knot signature $\{V, \Phi\}$ and uniform circular cross-section gives

$$M^* = \left(\frac{L^2}{2V} + \frac{\pi h^2}{L}\right)\Phi^2 \qquad \Rightarrow \qquad M^*|_{h=0} = \frac{\Phi^2}{2V}L^2, \tag{5}$$

where M^* is the constrained minimum energy of K, function of the knot length L and, in general, of the magnetic framing h given by the internal field twist; for zero-framed knots ($h = 0$), the constrained minimum takes the elementary form given by the equation on the right-hand side.

Now, for simplicity let us set $V = \Phi = 1$; then, from $V = 1 = \pi R^2 L$ (R radius of the tight knot cross-section) and

$$1 = \pi R^3\left(\frac{L}{R}\right) \qquad \Rightarrow \qquad R = \left(\frac{1}{\pi(L/R)}\right)^{1/3}, \tag{6}$$

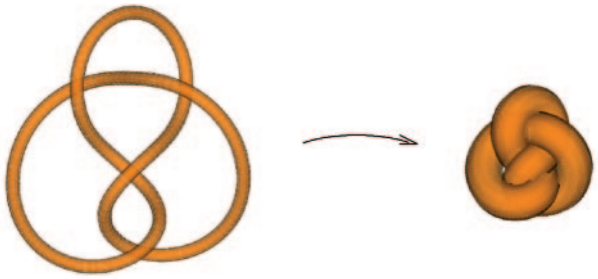

Fig. 2. – Relaxation of magnetic knot $K_{4.1}$ (on the left) to tight configuration (on the right): the energy minimum $M^* = M^*(L, h)$, given by eq. (5), depends on the tight knot length L and the twist parameter h.

we can express the tight knot length L in terms of the *ropelength* ratio L/R:

$$L = (L/R)\left(\frac{1}{\pi(L/R)}\right)^{1/3} = \left(\frac{(L/R)^2}{\pi}\right)^{1/3}. \tag{7}$$

Values of L/R for different knots in tight configuration can be calculated by the SONO algorithm developed by S. Pieranski and implemented by S. Przybyl, and they are readily available([1]). Thus, the constrained minimum energy of zero-framed knots can be explicitly calculated (see [12] for details). From a theoretical viewpoint, however, M^* could be further decreased by relaxing one (or more) of the constraints. For zero–framed knots one can indeed prove [13] that the absolute minimum energy $M_{\min}$ satisfies the relation

$$M_{\min} = \left(\frac{2}{\pi}\right)^{1/3} \frac{\Phi^2}{V^{1/3}} c_{\min}, \tag{8}$$

where $c_{\min}$ is the topological crossing number of the knot. By taking $V = \Phi = 1$ and combining the latter equation (8) with the second of (5), we have

$$M_{\min} = \left(\frac{2}{\pi}\right)^{1/3} c_{\min} \leq M^*|_{h=0} = \frac{1}{2}\left(\frac{(L/R)^2}{\pi}\right)^{2/3}, \tag{9}$$

that implies

$$\frac{L}{R} \geq (16\pi)^{1/4}(c_{\min})^{3/4} \approx 2.66(c_{\min})^{3/4}. \tag{10}$$

This result establishes a better bound on ropelength for knots of *any* $c_{\min}$ by improving Buck and Simon's [14] constant $(4\pi/11)^{3/4} \approx 1.10$. Recent work on *small* $c_{\min}$ knots, however, indicates that considerable progress can still be made: for the trefoil knot, for example, it is known that this constant may be ≈ 14.04 (see [15]). Since within each $c_{\min}$-family, there are several distinct knot types, eq. (8) cannot identify each knot

([1]) See the table at: `http://fizyka.phys.put.poznan.pl/~pieransk/TablesUpTo9.html`

energy level accurately. However, by re-writing the second equation of (5) in terms of ropelength, *i.e.*

$$M^* = \frac{(L/R)^{4/3}}{2\pi^{2/3}}\,, \tag{11}$$

we see that an improvement on constrained minima must come from work on the packing problem for knotted ropelength of given $c_{\min}$.

4. – Eigenvalue interpretation in terms of form factors of structural complexity

Work on structural complexity of physical systems aims at establishing relationships between mathematical and physical properties of such systems, relying on algebraic, geometric and topological information associated with dynamical and energetic aspects [1, 16]. For dynamical systems, critical point theory, eigenvalue analysis and bifurcation theory provide useful information [17], that can be exploited to quantify morphological complexity. Here we want to establish a new connection between eigenvalue information and structural complexity measures. For this let $\lambda_1 \geq \lambda_2 \geq \lambda_3 > 0$ be the three eigenvalues associated with a canonical form of a diffusion tensor field. To classify patterns several indices can be defined [18]; three of them are used to detect the isotropic distribution of field lines; these are

$$C_f = \frac{\lambda_1 - \lambda_2}{\sum_i \lambda_i}\,, \quad C_p = \frac{2(\lambda_2 - \lambda_3)}{\sum_i \lambda_i}\,, \quad C_s = \frac{3\lambda_3}{\sum_i \lambda_i}\,, \qquad (i = 1, 2, 3), \tag{12}$$

where C_f characterizes linear anisotropy (or filamentarity, or tubeness of field line distribution), C_p characterizes planar anisotropy (or planarity, or sheetness), and C_s characterizes spherical isotropy (or sphericity, or bulkiness of such distribution). Note that $C_f + C_p + C_s = 1$. Here we propose to interpret the three eigenvalues in terms of integral geometric measures by relating the three indices above to the so-called *shapefinders* used, for example, in cosmology [19] to qualify distribution of mass and energy in space. Let V and A denote the standard volume and bounding surface of a given distribution set $\mathcal{D}$, given by

$$V = \int_{\mathcal{D}} \mathrm{d}^3\mathbf{X}, \qquad A = \int_{\partial\mathcal{D}} \mathrm{d}^2\mathbf{X}, \tag{13}$$

and H and χ the global mean curvature and the Euler characteristic of the bounding surface $\partial\mathcal{D}$, given by

$$H = \frac{1}{2}\int_{\partial\mathcal{D}} \left(\frac{1}{R_1} + \frac{1}{R_2}\right) \mathrm{d}^2\mathbf{X}, \qquad \chi = \frac{1}{4\pi}\int_{\partial\mathcal{D}} \frac{1}{R_1 R_2}\, \mathrm{d}^2\mathbf{X}, \tag{14}$$

where R_1 and R_2 are the principal radii of curvature of $\partial\mathcal{D}$.

For convex distributions (*i.e.* $\mathcal{D}$ convex), the Minkowski functionals $V_0 = V$, $V_1 = A/6$, $V_2 = H/3\pi$ and $V_3 = \chi$ are all non-negative and may be used to define length L, width W and thickness T of the distribution set by the following relations:

$$L = \frac{H}{4\pi\chi}\,, \qquad W = \frac{A}{H}\,, \qquad T = \frac{3V}{A}\,, \tag{15}$$

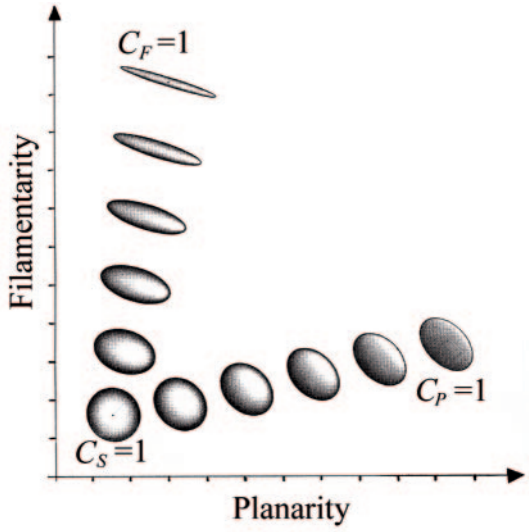

Fig. 3. – Balschke diagram of filamentarity (F) *vs.* planarity (P). Form factors define a triangular region.

where $L \geq W \geq T \geq 0$. Filamentarity F and planarity P are thus defined by

$$F = \frac{L-W}{L+W}\,, \qquad P = \frac{W-T}{W+T}\,, \tag{16}$$

to characterize tubeness and sheetness of $\mathcal{D}$. By comparing (12) with (16), and relying on the positiveness of the Minkowski functionals, we can re-define the anisotropy indices as

$$C_F = \frac{L-W}{L+W+T}\,, \qquad C_P = \frac{2(W-T)}{L+W+T}\,, \qquad C_S = \frac{3T}{L+W+T}\,, \tag{17}$$

with $C_F+C_P+C_S = 1$. As usual, the three indices can be interpreted as form factors in a Balschke diagram (see fig. 3) to characterize the morphology of the field line distribution. More interestingly, by comparing eqs. (12) and (15), we see that the three eigenvalues admit interpretation in terms of integral geometric properties of the distribution set, by taking

$$\lambda_1 \propto L, \qquad \lambda_2 \propto W, \qquad \lambda_3 \propto T, \tag{18}$$

so that eqs. (17) plainly coincide with eqs. (12) (note that all the parameters on the right-hand side have the dimensions of a length). Alternatively, information extracted from distribution sets of physical properties (mass, energy, etc.) can be interpreted, via eqs. (15) and (18), in terms of eigenvalues of a hypothetical dynamical system.

* * *

The author would like to thank R. Kusner for comments on the result of inequality (10). Financial support from 2006 PRIN project "Geometric Methods in the Theory of Non-Linear Waves and Applications" is kindly acknowledged.

REFERENCES

[1] Ricca R. L., *Structural complexity and dynamical systems*, in *Lectures on Topological Fluid Mechanics*, edited by Ricca R. L., *Lecture Notes in Mathematics*, Vol. **1973** (Springer, Berlin) 2009, pp. 167–186.
[2] Kida S., Takaoka M. and Hussain F., *Phys. Fluids A*, **1** (1989) 630.
[3] Boratav G. N., Pelz R. B. and Zabusky N., *Phys. Fluids A*, **4** (1992) 581.
[4] Ricca R. L. and Moffatt H. K., *The helicity of a knotted vortex filament*, in *Topological Aspects of the Dynamics of Fluids and Plasmas*, edited by Moffatt H. K. *et al.* (Kluwer, Dordrecht) 1992, pp. 225–236.
[5] Aref H. and Zawadzki I., *Nature*, **354** (1991) 50.
[6] Widnall S. E. and Sullivan J. P., *Proc. R. Soc. London, Ser. A*, **322** (1973) 335.
[7] Saffman P. G., *Vortex Dynamics* (Cambridge University Press) 1992.
[8] Arms R. J. and Hama F. R., *Phys. Fluids*, **8** (1965) 553.
[9] Ricca R. L., Samuels D. C. and Barenghi C. F., *J. Fluid Mech.*, **391** (1999) 29.
[10] Moffatt H. K., *Nature*, **347** (1990) 367.
[11] Cantarella J., Kusner R. B. and Sullivan J. M., *Invent. Math.*, **150** (2002) 257.
[12] Maggioni F. and Ricca R. L., to be published in *Proc. R. Soc. London, Ser. A* (doi: 10.1098/rspa.2008.0536).
[13] Ricca R. L., *Proc. R. Soc. London, Ser. A*, **464** (2008) 293.
[14] Buck G. and Simon J., *Topol. Appl.*, **91** (1999) 245.
[15] Baranska J., Pieranski P. and Przybyl S., *Phys. Rev E*, **70** (2004) 051810.
[16] Ricca R. L., *Structural complexity*, in *Encyclopedia of Nonlinear Science*, edited by Scott A. (Routledge, New York and London) 2005, pp. 885–887.
[17] Chong M. S., Perry A. E. and Cantwell B. J., *Phys. Fluids A*, **2** (1990) 765.
[18] Vilanova A., Zhang S., Kindlmann G. and Laidlaw D., *An introduction to visualization of diffusion tensor imaging and its applications*, in *Visualization and Processing of Tensor Fields*, edited by Weickert J. and Hagen H. (Springer, Berlin) 2006, pp. 121–153.
[19] Sahni V., Sathyaprakash B. S. and Shandarin S. F., *Astrophys. J.*, **495** (1998) L5.